applied optics

Influence of blood pulsation on diagnostic volume in pulse oximetry and photoplethysmography measurements

Viktor Dremin,[1,2,8] Evgeny Zherebtsov,[1,2] Alexander Bykov,[1] Alexey Popov,[1] Alexander Doronin,[3] and Igor Meglinski[1,4,5,6,7,*]

[1] *Opto-Electronics and Measurement Techniques Unit, Faculty of Information Technology and Electrical Engineering, University of Oulu, Oulu 90570, Finland*
[2] *Research & Development Center of Biomedical Photonics, Orel State University, Orel 302026, Russia*
[3] *Computer Graphics Group, School of Engineering and Computer Science, Victoria University of Wellington, Wellington 6140, New Zealand*
[4] *Interdisciplinary Laboratory of Biophotonics, National Research Tomsk State University, Tomsk 634050, Russia*
[5] *Institute of Engineering Physics for Biomedicine (PhysBio), National Research Nuclear University (MEPhI), Moscow 115409, Russia*
[6] *Aston Institute of Materials Research, School of Engineering & Applied Science, Aston University, Birmingham B4 7ET, UK*
[7] *School of Life & Health Sciences, Aston University, Birmingham B4 7ET, UK*
[8] *e-mail: viktor.dremin@oulu.fi*
Corresponding author: i.meglinski@aston.ac.uk

Recent advances in the development of ultra-compact semiconductor lasers and technology of printed flexible hybrid electronics have opened broad perspectives for the design of new pulse oximetry and photoplethysmography devices. Conceptual design of optical diagnostic devices requires careful selection of various technical parameters, including spectral range; polarization and intensity of incident light; actual size, geometry, and sensitivity of the detector; and mutual position of the source and detector on the surface of skin. In the current study utilizing a unified Monte Carlo computational tool, we explore the variations in diagnostic volume due to arterial blood pulsation for typical transmitted and back-scattered probing configurations in a human finger. The results of computational studies show that the variations in diagnostic volumes due to arterial pulse wave are notably (up to 45%) different in visible and near-infrared spectral ranges in both transmitted and back-scattered probing geometries. While these variations are acceptable for relative measurements in pulse oximetry and/or photoplethysmography, for absolute measurements, an alignment normalization of diagnostic volume is required and can be done by a computational approach utilized in the framework of the current study. © 2019 Optical Society of America

1. INTRODUCTION

Nowadays, diffuse light spectroscopy is used extensively in quantitative characterization of biological tissues [1]. The diffuse reflective spectra of skin and other biological tissues contain valuable information about concentration and spatial distribution of major chromophores, such as oxy- and deoxyhemoglobin, melanin, bilirubin, carotene, water, etc. The use of light in visible (400–700 nm) and/or near-infrared (NIR, 700–1400 nm) spectral ranges provides an opportunity to conduct such measurements non-invasively and in real time [2].

Diffuse reflectance measurements are used in a number of diagnostic technologies in the form of steady-state diffuse reflectance spectroscopy [3] in visible and NIR ranges, diffusing-wave spectroscopy (also called diffuse correlation spectroscopy) [4,5], fluorescence spectroscopy [6,7], laser

Doppler flowmetry (LDF) [8], photoplethysmography (PPG) [9], pulse oximetry [10], etc., as well as spatially resolved hyperspectral methods based on the described spectroscopic technologies [2,11]. Novel diagnostic wearable devices open new horizons for application of the different modalities of diffuse spectroscopy. This group of measurement techniques ensures simplicity of realization of such devices and their compactness [12].

An actual design of optical/NIR probe for a particular diagnostic application requires careful selection of optimal source–detector parameters and their mutual position on the skin surface. The spatial distribution of detector depth sensitivity within biological tissue, known also as diagnostic or sampling volume, is typically used for assessment of the efficiency of experimental detection [13,14]. The knowledge of diagnostic volume is also extremely important in terms of

functional interpretation of the results with respect to physiological variations occurring within biological tissues.

In general, the sampling volume approximates a region of a biological tissue with a significant number of effective optical paths of the detected photons [15]. The PPG approach provides information on a particular type of vascular bed involved in formation of the detected signal [16,17]. Technical parameters of the employed diagnostic system (probing geometry and wavelength of probing radiation), as well as optical parameters of the medium, are major factors that influence the resolution and light distribution in biological tissues. When carrying out optical measurements, it is necessary to take into account the presence of various physiological and neurophysiological oscillatory processes in the blood microcirculation system [18]. The strongest fluctuations in blood perfusion of tissues are caused by changes in the arterial pulse waves. Recently, pronounced pulse oscillations were detected even in the capillary bed [19]. Moreover, the respiratory, myogenic, neurogenic, and endothelial mechanisms of regulation can also modulate blood flow. Therefore, parameters such as blood volume and oxygen saturation level are also not constant [20]. Consequently, any single measurement can occur at both the maximum and minimum of the amplitude of the oscillations of the measured parameters, which significantly complicates the interpretation of such "one-off" indicators [21]. On this basis, an alteration of the blood volume fraction, as well as oxygen saturation level, can affect the size of the sampling volume. The absolute quantified analysis of collected reflectance spectra of skin is complicated due to the fact that the blood content of tissues can vary in the spatial and volumetric distribution. These measurements require understanding the vascular beds, which are primarily responsible for the variations in the detected signal.

Thus, the aim of the current study is to explore the variations in diagnosis volume caused by arterial blood pulsation, as well as to evaluate the effective depth of penetration of probing light at different spectral bands. One of the possible ways to formalize quantitative evaluation of the sampling volume is the assessment of spatial distribution of detector depth sensitivity. The sampling volume is formed by the so-called effective optical paths, i.e., the paths that probing light propagates from the source to the detector. The quantity is defined as the gradient of the optical density with respect to absorption coefficient μ_a at each pixel r in the scattering medium [15]:

$$Q(r) = -\frac{\partial}{\partial \mu_a(r)} \ln\left(\frac{I}{I_0}\right), \qquad (1)$$

where $\mu_a(r)$ is the absorption coefficient, I_0 is the incident intensity of probe radiation, and I is the intensity of detected radiation.

Here, it should be pointed out that changes in the sampling volume are inseparably linked to changes in the value of the signal on the detector. For example, an increase in blood volume fraction of biological tissue leads to an increase in its optical absorption properties and as a consequence, to a decrease in the signal registered by the detector.

Radiation transfer theory (RTE) is widely applied to describe light propagation within turbid tissue-like scattering media [22]. The main problem of the RTE solution is to determine the diffuse component of light intensity, since the scattering of photons is random. Several approximations have been proposed, including the theory of probabilistic photon migration [23], Kubelka–Munk theory [24], diffusion approximation [25], and their combinations. Analytic models have an advantage of providing a relatively simple form of the theoretical solution. However, they require certain boundary conditions that very often cannot be defined due to the complexity of the internal structure of biological tissues. In fact, there is a "gold standard" approach, which involves numerical solution of the RTE known as the Monte Carlo (MC) method [26,27]. The MC technique is able to provide a realistic distribution of light propagation in biological tissues.

2. MONTE CARLO MODELING

MC simulation consists of a sequential generation of trajectories of so-called photon packets from the site of photons' entrance into the medium ("source") to the area where the photon leaves the medium ("detector"). In this study, a GPU-accelerated MC-distributed online computational platform that implements an object-oriented concept [27,28] was used for a routine simulation of detector depth sensitivity (known also as "sampling volume" or diagnostic volume). This approach allows for representation of photon packets and tissue structural components as the objects and defines their mutual interactions. Thus, the object–photon packet propagates through a turbid-tissue-like scattering medium, represented as a set of objects, such as cells, blood vessels, collagen fibers, etc., and interacts with them. The object-based representation of the turbid medium makes it possible to develop realistic models of various biological tissues presenting 3D spatial variations in structural malformations associated with a particular disease.

Thus, the MC model of biological tissue is represented as a 3D grid, divided into individual (elementary) voxels. To assess the probability density function of the effective optical paths, each photon packet trajectory is processed voxel by voxel, and the sampling volume in a particular voxel is calculated as

$$Q(r) = -\frac{\partial}{\partial \mu_a(r)} \ln\left(\frac{I}{I_0}\right) = \frac{\sum_{i=1}^{N_{ph}} l_i(r) W_{di}}{l_0 \sum_{i=1}^{N_{ph}} W_{di}}, \qquad (2)$$

where W_{di} corresponds to the final weight of the i-th detected photon, N_{ph} is the number of photon packets satisfying the detection conditions, l_i is a pathlength of the i-th photon packet in a pixel with a center located at r, and l_0 is the size of the pixel.

When a photon packet is registered by the detector, its final statistical weight is found according to

$$W_d = W_0 \exp\left(-\sum_k \mu_{ak} l_k\right). \qquad (3)$$

Here, W_d corresponds to the statistical weight of the detected photon packet, μ_{ak} is the absorption coefficient of the k-th pixel (the medium is represented by a number of pixels), l_k is the total path length of the photon packet in the k-th pixel, and $W_0 = 1$ is the initial statistical weight of the photon packet.
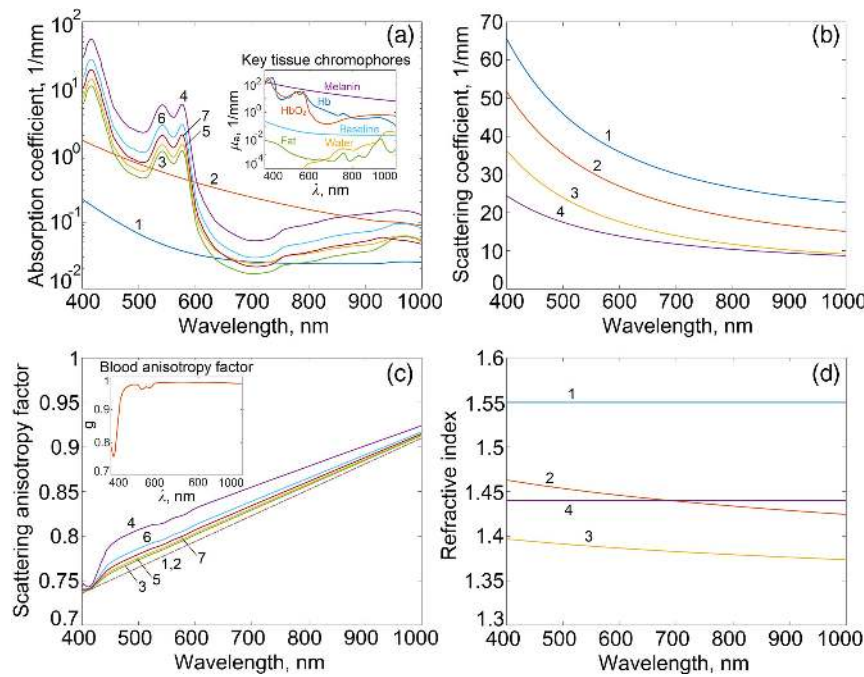
Fig. 1.   (a) Absorption coefficients of tissue layers: 1–*Stratum corneum*, 2–epidermis, 3–papillary dermis, 4–upper blood net dermis, 5–reticular dermis, 6–deep blood net dermis, 7–subcutaneous tissue. (b) Scattering coefficients: 1–*Stratum corneum*, 2–epidermis, 3–dermis, 4–subcutaneous fat. (c) Scattering anisotropy factor: numerical designations correspond to the designations described for the absorption coefficients. (d) Refractive index: numerical designations correspond to the designations described for the scattering coefficients. Optical properties were derived from a number of sources described in the text.

For the quantitative assessment, we consider a cross section of $Q(r)$ in terms of x and z coordinates ($Q(x, z)$), where x is the horizontal axis referring to the center-to-center of the source and detector position, and z is the depth. The sampling volume is estimated up to 10^{-3} of the detected intensity of light, which corresponds to the dynamic range of the conventional detectors available commercially [1]. A modified multilayered tissue model was used to assess the sampling volume for the reflectance and transmittance experimental systems typically used in pulse oximetry and PPG measurements. This skin model employed in our study has been used and tested by the authors previously [10,15,29,30]. A good agreement with the experimental data has been demonstrated. This type of model takes into account variations in the absorption and scattering properties, including depth variations in blood and melanin content, blood oxygen saturation, hematocrit, and water content within the skin. The other input parameters of the model are the size of the light source and the detector, the distance between them, the tilt of the light source, and the detector's numerical aperture. The thicknesses of the layers were selected based on the average values following earlier publications [17,31,32] aimed at computational modeling of light propagation in the skin with a similar multilayered skin model. The absorption property of biological tissue usually refers to the value of average absorption coefficient μ_a, since the molecular composition of the tissue is not well specified. Thus, the total absorption of the tissue can be expressed through the volume fraction of the tissue component C_i and the absorption coefficient of this component μ_{ai}:

$$\mu_a(\lambda) = \sum_i C_i \mu_{ai}(\lambda). \tag{4}$$

Thus, the absorption coefficients of the tissue layers [Fig. 1(a)] were calculated by taking into account the concentration of blood C_{blood}, oxygen saturation S, water content C_{water}, hematocrit Ht, melanin fraction C_{mel}, and fat content C_{fat}.

The scattering coefficient of each layer within the current study [Fig. 1(b)] is represented by a combination of Mie and Rayleigh theories [33], derived from a number of sources [34–37]. The scattering anisotropy factor g for each layer [Fig. 1(c)] was extrapolated depending on the blood concentration, and the reference experimental data for skin [38] and blood [39]. The refractive index is considering a functional dependence on the wavelength [Fig. 1(d)] and for each of the layers was obtained from a number of sources [40–42]. The optical properties of the bone were taken into account in modeling of the diffuse transmission following the optical parameters published earlier [10,43–45].

A. Back-Scattered Probing Configuration

A previously reported theoretical model of the formation of the PPG reflectance signal originates from the compression of skin tissue components due to arterial expansion and the resulting changes in the dermal opto-mechanical properties [46,47]. We represent the pulse wave by an addition of an extra arterial layer within the upper and deep blood net dermis [48]. This approach allows to take into account the change not only in absorption, but also in scattering.

The thickness of the arterial layers varied by 0–25 μm and 0–50 μm, respectively, and then the papillary dermis and reticular dermis were compressed to compensate for the overall
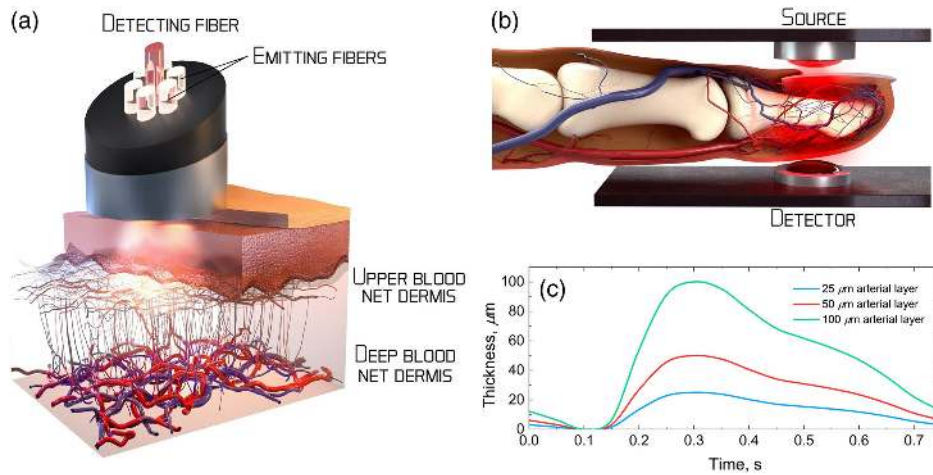
Fig. 2. Typical layout of diffuse (a) reflectance and (b) transmittance measurements and skin tissue layers; (c) PPG function of changes in the arterial layer thickness taken into account in the MC model.

Table 1. Parameters of the Diffuse Reflectance Model [30,36,39]

Layer	Thickness, μm	Blood Volume Fraction, C_{blood}, %
Stratum corneum	20	0
Epidermis	80	0
Papillary dermis	100	5
Upper blood net dermis	80	20
Reticular dermis	1620	4
Deep blood net dermis	200	10
Subcutaneous fat	6000	7

change in thickness. When the thickness of the papillary dermis and reticular dermis decreased, the volume fraction of blood increased proportionally in order to maintain the same total amount of blood volume in these two layers, before changing the thickness of the added arterial layers. Alteration of the arterial layer thickness was completed using the PPG function. The maximum thickness of the additional arterial layer corresponded to systole and the minimum to diastole [Fig. 2(c)].

Diffuse reflectance measurements can be performed by different instruments, e.g., with spectrometers with a diffraction grating and fiber-optical probes being the most common [Fig. 2(a)]. In this study, the sampling volume for the diffuse reflectance QR400 series probe (Ocean Optics, Inc., USA) was modeled and analyzed. The probe has six emitting fibers and one collecting fiber. Both types of fibers are 400 μm in diameter with a numerical aperture of 0.22. Separation between the collecting and emitting fibers is set as 480 μm. To assess the sampling volume, a seven-layer model of skin was used. The main parameters of the model are presented in Table 1.

The calculations were carried out for the following wavelengths: 450 nm, 532 nm, 660 nm, 800 nm, 860 nm, and 940 nm.

B. Transmittance Probing Configuration

Pulse oximeters are popular devices that realize the measurement of diffuse transmission [Fig. 2(b)]. A typical design of a pulse oximetric sensor is a light source or matrix with several sources and a radiation receiver. The recorded signal represents the radiation transmitted through the tissue. For the purpose of simulation, the source and detector sizes of 1 mm and 3 mm were set, respectively. To assess sampling volume an 18-layer model of a finger 12 mm thick was used. The main parameters of the model are outlined in Table 2.

The calculations were carried out for 660 nm and 940 nm. When simulating transmission in addition to the pulsating

Table 2. Parameters of the Diffuse Transmittance Model

Layer	Thickness, μm	Blood Volume Fraction, C_{blood}, %
Nail	500	0
Papillary dermis	100	5
Upper blood net dermis	80	20
Reticular dermis	600	4
Deep blood net dermis	200	10
Subcutaneous fat	1050	7
Arterial layer	1000	100
Subcutaneous fat and muscle	1050	7
Bone tissue	2500	2
Subcutaneous fat and muscle	1300	7
Arterial layer	1000	100
Subcutaneous fat	1540	7
Deep blood net dermis	200	10
Reticular dermis	600	4
Upper blood net dermis	80	20
Papillary dermis	100	5
Epidermis	80	0
Stratum corneum	20	0

layers of the upper and deep blood net dermis, an additional pulsating layer was added to the arterial layer of the subcutaneous tissue. Its thickness varied within 0–100 μm. In this study, sampling volume was calculated on the basis of 10^9 detected photon packets.

3. RESULTS

The results of MC modeling of the sampling volume for the back-scattered diffuse reflectance source–detector configuration [Fig. 2(a)] for the plane passing through the center-to-center of the receiving and detecting fibers are presented in Fig. 3.

These results are also presented in the form of animated graphs showing the dynamics of sampling volume changes due to arterial pulse wave propagation (see Visualization 1). It is clearly seen that for 450 nm, the probing depth does not exceed 700 μm, whereas for the NIR spectral range, it reaches up to 2.5–3 mm. The results show that in blue and green spectral ranges, the epidermis, papillary dermis layer, upper blood net dermis, and a very shallow part of the reticular dermis are probed, whereas in the red-NIR band of the spectrum, the probing light is able to sense even subcutaneous tissues.
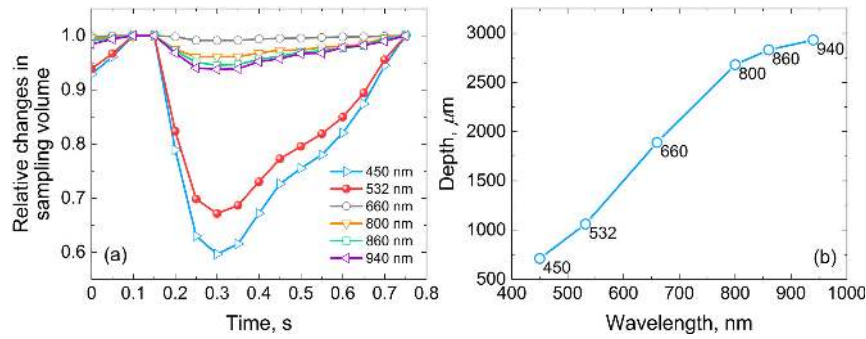
The relative changes in sampling volume for different wavelengths during the arterial pulse wave period are presented in Fig. 4(a). As one can see, an increase in blood content can lead to a significant change in the sampling volume (45% at 450 nm and 37% at 532 nm). The relative changes were evaluated by the values of the sampling volume between systole and diastole.

The most resistant to changes in blood content is the 660 nm light (less than 1%). The light of 940 nm is often used in conjunction with 660 nm light in pulse oximetry sensors. Meanwhile, the sampling volume at 940 nm light is notably distinguished compared to the sampling volume at 660 nm, and is the subject of significant variations along the arterial pulse wave (7%). At the same time, taking into account the larger sampling volume for the red-NIR band, its absolute changes are comparable for the visible and NIR bands. For example, for 450 nm sampling volume, changes are 0.24 mm³, and for 940 nm, they are 0.21 mm³.

In comparison to the back-scattered diffuse reflectance probing configuration (Fig. 3), the results of sampling volume modeling for the diffuse transmittance configuration are presented in Figs. 5(a) and 5(b); see also these results in the form of animated graphs (Visualization 2).
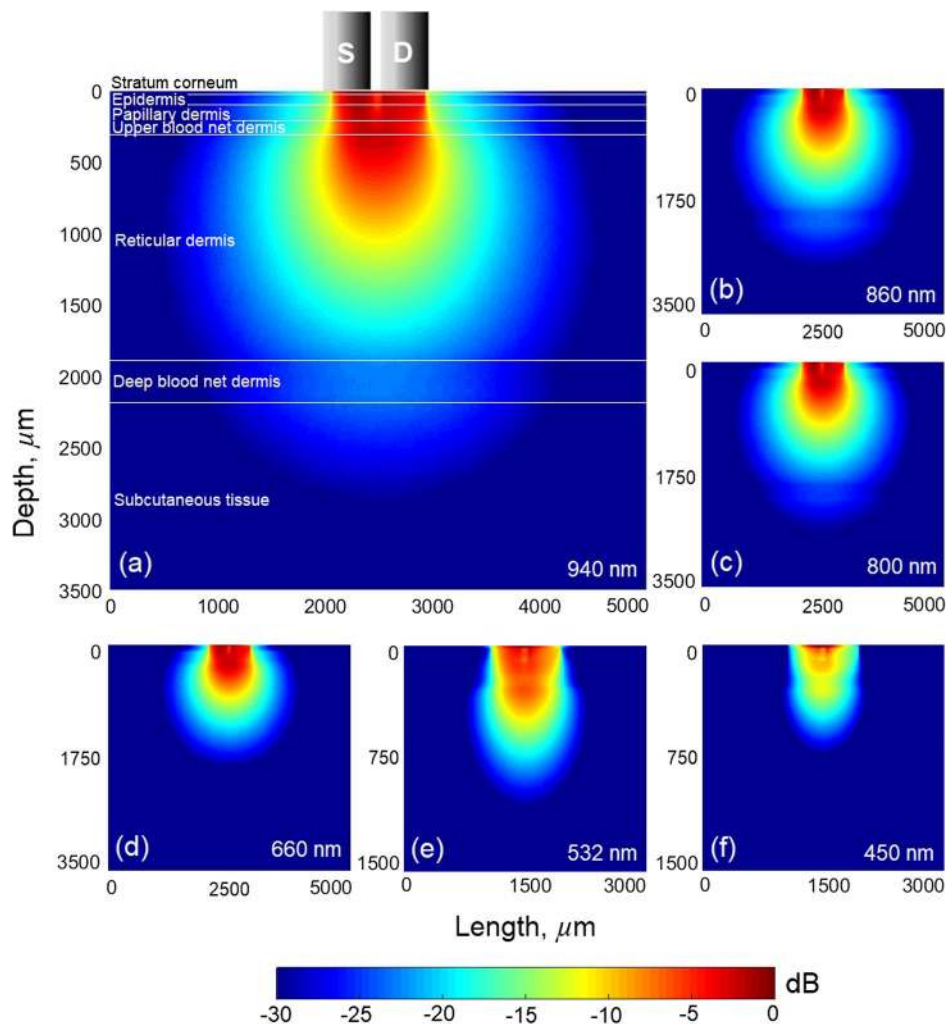
Fig. 3. Sampling volume for the back-scattered diffuse reflectance probe, schematically presented in Fig. 2(a). The wavelengths of light used in the modeling are: (a) 940 nm, (b) 860 nm, (c) 800 nm, (d) 660 nm, (e) 532 nm, and (f) 450 nm (see Visualization 1).

Fig. 4. (a) Relative changes in sampling volume distribution for different light wavelengths during the arterial wave pulse period; (b) light penetration depth at 10^{-3} of the incident light intensity.
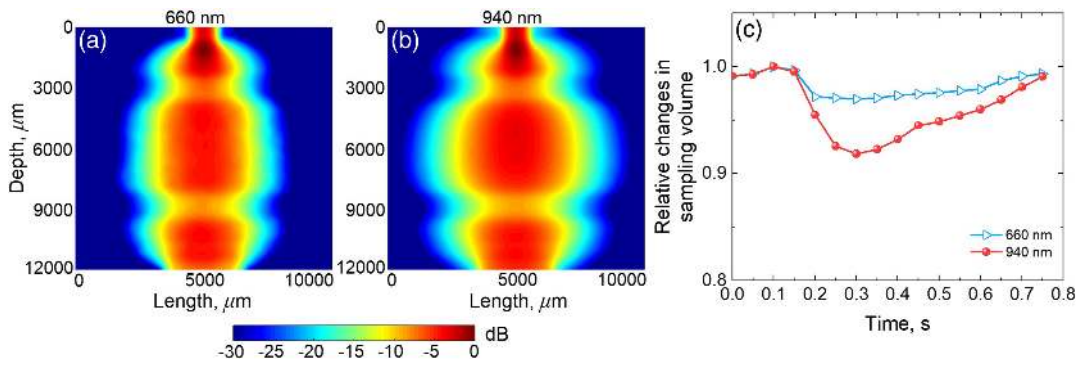
Fig. 5. Sampling volume obtained for the transmittance configuration of the source and detector, schematically presented in Fig. 2(b) for the wavelengths (a) 660 nm and (b) 940 nm (see Visualization 2). (c) Relative changes in sampling volume.

As one can see, at 660 nm, the sampling volume [Fig. 5(a)] shows the largest variations compared to the back-scattered diffuse reflectance configuration (3%) presented in Fig. 3. Arguably, this is due to the large absorbing properties of the arterial layer of the subcutaneous tissue. Changes in sampling volume at 940 nm light reach up to 10%.

4. DISCUSSION

In general, a phenomenological relationship for the sampling volume and the rise in effective penetration depth of light with the increasing wavelength can be deduced [Fig. 4(b)]. It should be pointed out that for the probing of deep vascular plexuses in the skin, the most optimal range of wavelengths is revealed to be between 800 nm and 970 nm, since the diagnostic volumes, as well as the light penetration depths are quantitatively similar in this range of spectrum (Figs. 3 and 4).

The results of sampling volume modeling show that pulse oximetry or PPG signal formation is significantly dependent on the contribution of venous or arterial vascular beds. As the blood volume and oxygen saturation of blood in the particular vascular bed in human skin can vary significantly along the arterial pulse wave propagation, for diagnostic purposes, an averaging of measured signal recorded during a certain period of time is required. From this point of view, in light of further development of this approach, it seems quite logical to evaluate the average value of each variable, as well as to monitor frequency and amplitude of their oscillations [19,49,50].

It also should be pointed out here that in addition to the dynamic range of the detector, the sampling volume and the effective probing depth are influenced greatly by a specific source–detector configuration. In particular, the detector depth sensitivity is highly influenced by the source–detector separation [13–15]. The probe also is required to be properly positioned on the skin surface to prevent uncertainties associated with the mechanical pressure that eliminates the signal from superficial capillary loops [51,52] and introduces a systematic error in the interpretation of the experimental results.

While PPG and pulse oximetry are widely used in biomedical optics, currently available devices are based on an empirical calibration that does not work properly, especially for the low oxygen saturation of blood [53,54]. Therefore, currently available pulse oximetry and/or PPG devices are used for relative measurements only, whereas for absolute measurements, an alignment normalization of diagnostic volumes is required, e.g., by using the MC approach utilized in the current study. Thus, the accuracy of pulse oximetry/PPG devices can be significantly improved and extended for absolute measurements of oxygen saturation of blood within skin tissues for variable sensor geometry. This can be extremely useful for oxygen saturation measurement in critically ill patients because the empirical calibration of pulse oximeters is based on examinations of healthy volunteers and is not necessarily applicable to critically ill patients or for fetal pulse oximetry—a new blood flow diagnostic paradigm where taking into account the low oxygen saturation of blood is critical [55].

However, the absolute quantified analysis of collected reflectance spectra of skin is complicated due to the fact that the blood content and oxygen saturation level are not constant and can vary in spatial distribution. Changes in the sampling volume during pulse influence the contribution of different types of vessels of venous or arterial vascular beds to the detected signal. This affects the measured values of oxygen saturation of blood. While these variations are acceptable for relative measurements in pulse oximetry and/or PPG, for the absolute measurements, an alignment normalization of diagnostic volume is required and can be done by a computational approach utilized in the framework of the current study.

The possibility of applying the unified MC computational tool to theoretical evaluation of the calibration curve for pulse oximetry was shown in the works [10,56]. The results obtained in the current study indicate the need to take into account the effect of changes in the sampling volume on the recorded signals when calculating the calibration curve. The use of correction factors will compensate for the inaccuracy in the measurement of blood oxygenation associated with changes in the sampling volume. This will improve the theoretical calibration approach in pulse oximetry/PPG techniques.

5. CONCLUSION

To sum up, utilizing a unified Monte Carlo computational tool, we explore the variations in diagnostic volume due to heart pulse wave for typical transmitted and back-scattered probing configurations used at the pulse oximetry and PPG measurements in a human finger. The results of computational studies, presented in the form of 2D maps of sampling volume $Q(x, z)$, show that the variations in diagnostic volumes due to arterial pulse wave are notably (from 1% up to 45%) different in visible and NIR spectral ranges in both transmitted and back-scattered probing geometries. The developed MC-based computational approach for assessment of sampling volume is available online (see [28]) and can be routinely used for quantitative assessment of detector depth sensitivity of various back-scattered diffuse reflected and transmitted source–detector configurations. Development of PPG and pulse oximetry sensors includes the selection of optimal wavelengths, source and detector configuration, and other technical parameters. The use of the MC technique utilized in the current study can contribute significantly to the design of such sensors with a primary aim to achieve better accuracy in measured signal. The developed technique can also help in the interpretation of physiological variations in blood content, oxygen saturation, malformations in anatomical structures, and other factors associated with particular diseases and/or treatment procedures.

Disclosures. The authors declare that there are no conflicts of interest related to this paper.

REFERENCES

1. V. V. Tuchin, *Handbook of Optical Biomedical Diagnostics, Second Edition, Volume 2: Methods* (SPIE, 2016).
2. E. Zherebtsov, V. Dremin, A. Popov, A. Doronin, D. Kurakina, M. Kirillin, I. Meglinski, and A. Bykov, "Hyperspectral imaging of human skin aided by artificial neural networks," Biomed. Opt. Express **10**, 3545–3559 (2019).
3. G. Zonios and A. Dimou, "Light scattering spectroscopy of human skin in vivo," Opt. Express **17**, 1256–1267 (2009).
4. I. V. Meglinski, V. V. Kalchenko, Y. L. Kuznetsov, B. I. Kuznik, and V. V. Tuchin, "Towards the nature of biological zero in the dynamic light scattering diagnostic modalities," Dokl. Phys. **58**, 323–326 (2013).
5. I. Meglinski and V. V. Tuchin, "Diffusing wave spectroscopy: application for blood diagnostics," in *Handbook of Coherent-Domain Optical Methods: Biomedical Diagnostics, Environmental Monitoring, and Materials Science*, V. V. Tuchin, ed. (Springer, 2013), pp. 149–166.
6. A. Dunaev, V. Dremin, E. Zherebtsov, I. Rafailov, K. Litvinova, S. Palmer, N. Stewart, S. Sokolovski, and E. Rafailov, "Individual variability analysis of fluorescence parameters measured in skin with different levels of nutritive blood flow," Med. Eng. Phys. **37**, 574–583 (2015).
7. M. A. Mycek and B. W. Pogue, *Handbook of Biomedical Fluorescence* (Taylor & Francis, 2003).
8. M. J. Leahy and G. E. Nilsson, "Laser Doppler flowmetry for assessment of tissue microcirculation: 30 years to clinical acceptance," Proc. SPIE **7563**, 75630E (2010).
9. Y. Sun and N. Thakor, "Photoplethysmography revisited: from contact to noncontact, from point to imaging," IEEE Trans. Biomed. Eng. **63**, 463–477 (2016).
10. A. Doronin, I. Fine, and I. Meglinski, "Assessment of the calibration curve for transmittance pulse-oximetry," Laser Phys. **21**, 1972–1977 (2011).
11. G. Lu and B. Fei, "Medical hyperspectral imaging: a review," J. Biomed. Opt. **19**, 10901–10924 (2014).
12. E. A. Zherebtsov, E. V. Zharkikh, I. Kozlov, A. I. Zherebtsova, Y. I. Loktionova, N. B. Chichkov, I. E. Rafailov, V. V. Sidorov, S. G. Sokolovski, A. V. Dunaev, and E. U. Rafailov, "Novel wearable VCSEL-based sensors for multipoint measurements of blood perfusion," Proc. SPIE **10877**, 1087708 (2019).

13. I. V. Meglinski and S. D. Matcher, "Analysis of the spatial distribution of detector sensitivity in a multilayer randomly inhomogeneous medium with strong light scattering and absorption by the Monte Carlo method," Opt. Spectrosc. **91**, 654–659 (2001).

14. I. V. Meglinskii, A. N. Bashkatov, E. A. Genina, D. Y. Churmakov, and V. V. Tuchin, "Study of the possibility of increasing the probing depth by the method of reflection confocal microscopy upon immersion clearing of near-surface human skin layers," Quantum Electron. **32**, 875–882 (2002).

15. I. V. Meglinsky and S. J. Matcher, "Modelling the sampling volume for skin blood oxygenation measurements," Med. Biol. Eng. Comput. **39**, 44–50 (2001).

16. M. V. Volkov, N. B. Margaryants, A. V. Potemkin, M. A. Volynsky, I. P. Gurov, O. V. Mamontov, and A. A. Kamshilin, "Video capillaroscopy clarifies mechanism of the photoplethysmographic waveform appearance," Sci. Rep. **7**, 13298 (2017).

17. A. V. Moço, S. Stuijk, and G. de Haan, "New insights into the origin of remote PPG signals in visible light and infrared," Sci. Rep. **8**, 8501 (2018).

18. A. Stefanovska, M. Bracic, and H. D. Kvernmo, "Wavelet analysis of oscillations in the peripheral blood circulation measured by laser Doppler technique," IEEE Trans. Biomed. Eng. **46**, 1230–1239 (1999).

19. V. Dremin, I. Kozlov, M. Volkov, N. Margaryants, A. Potemkin, E. Zherebtsov, A. Dunaev, and I. Gurov, "Dynamic evaluation of blood flow microcirculation by combined use of the laser Doppler flowmetry and high-speed videocapillaroscopy methods," J. Biophoton. **12**, e201800317 (2019).

20. A. V. Dunaev, V. V. Sidorov, A. I. Krupatkin, I. E. Rafailov, S. G. Palmer, N. A. Stewart, S. G. Sokolovski, and E. U. Rafailov, "Investigating tissue respiration and skin microhaemocirculation under adaptive changes and the synchronization of blood flow and oxygen saturation rhythms," Physiol. Meas. **35**, 607–621 (2014).

21. C. E. Thorn, S. J. Matcher, I. V. Meglinski, and A. C. Shore, "Is mean blood saturation a useful marker of tissue oxygenation?" Am. J. Physiol. Heart Circ. Physiol. **296**, H1289–H1295 (2009).

22. A. Ishimaru, *Wave Propagation and Scattering in Random Media* (Elsevier, 1978).

23. J. Wu, F. Partovi, M. S. Field, and R. P. Rava, "Diffuse reflectance from turbid media: an analytical model of photon migration," Appl. Opt. **32**, 1115–1121 (1993).

24. A. A. Kokhanovsky, "Physical interpretation and accuracy of the Kubelka–Munk theory," J. Phys. D **40**, 2210–2216 (2007).

25. W. M. Star, "Diffusion theory of light transport," in *Optical-Thermal Response of Laser-Irradiated Tissue* (Springer, 1995), pp. 131–206.

26. S. Jacques and L. Wang, "Monte Carlo modeling of light transport in tissues," in *Optical-Thermal Response of Laser-Irradiated Tissues* (Springer, 1995), pp. 73–100.

27. A. Doronin and I. Meglinski, "Online object oriented Monte Carlo computational tool for the needs of biomedical optics," Biomed. Opt. Express **2**, 2461–2469 (2011).

28. "Cloud based Monte Carlo tool for photon transport," www.biophotonics.fi, Accessed 2019-08-10.

29. S. J. Matcher and I. V. Meglinski, "Quantitative assessment of skin layers absorption and skin reflectance spectra simulation in the visible and near-infrared spectral regions," Physiol. Meas. **23**, 741–753 (2002).

30. G. I. Petrov, A. Doronin, H. T. Whelan, I. Meglinski, and V. V. Yakovlev, "Human tissue color as viewed in high dynamic range optical spectral transmission measurements," Biomed. Opt. Express **3**, 2154–2161 (2012).

31. I. Meglinski, A. Doronin, A. Bashkatov, E. Genina, and V. Tuchin, "Dermal component–based optical modeling of skin translucency: impact on skin color," in *Computational Biophysics of the Skin* (Pan Stanford, 2014), pp. 25–61.

32. Y. Masuda, Y. Ogura, Y. Inagaki, T. Yasui, and Y. Aizu, "Analysis of the influence of collagen fibres in the dermis on skin optical reflectance by Monte Carlo simulation in a nine-layered skin model," Skin Res. Technol. **24**, 248–255 (2018).

33. I. S. Saidi, S. L. Jacques, and F. K. Tittel, "Mie and Rayleigh modeling of visible-light scattering in neonatal skin," Appl. Opt. **34**, 7410–7418 (1995).

34. E. Salomatina, B. Jiang, J. Novak, and A. N. Yaroslavsky, "Optical properties of normal and cancerous human skin in the visible and near-infrared spectral range," J. Biomed. Opt. **11**, 064026 (2006).

35. A. N. Bashkatov, E. A. Genina, and V. V. Tuchin, "Optical properties of skin, subcutaneous, and muscle tissues: a review," J. Innov. Opt. Health Sci. **04**, 9–38 (2011).

36. S. L. Jacques, "Optical properties of biological tissues: a review," Phys. Med. Biol. **58**, R37–R61 (2013).

37. S.-H. Tseng, A. Grant, and A. J. Durkin, "In vivo determination of skin near-infrared optical properties using diffuse optical spectroscopy," J. Biomed. Opt. **13**, 014016 (2008).

38. M. J. van Gemert, S. L. Jacques, H. J. Sterenborg, and W. M. Star, "Skin optics," IEEE Trans. Biomed. Eng. **36**, 1146–1154 (1989).

39. N. Bosschaart, G. J. Edelman, M. C. G. Aalders, T. G. van Leeuwen, and D. J. Faber, "A literature review and novel theoretical approach on the optical properties of whole blood," Laser Med. Sci. **29**, 453–479 (2014).

40. F. A. Duck, *Physical Properties of Tissues* (Elsevier, 1990).

41. H. Ding, J. Q. Lu, W. A. Wooden, P. J. Kragel, X.-H. Hu, and X. Hu, "Refractive indices of human skin tissues at eight wavelengths and estimated dispersion relations between 300 and 1600 nm," Phys. Med. Biol. **51**, 1479–1489 (2006).

42. G. J. Muller and A. Roggan, *Laser-Induced Interstitial Thermotherapy* (SPIE, 1995).

43. A. Pifferi, A. Torricelli, P. Taroni, A. Bassi, E. Chikoidze, E. Giambattistelli, and R. Cubeddu, "Optical biopsy of bone tissue: a step toward the diagnosis of bone pathologies," J. Biomed. Opt. **9**, 474–480 (2004).

44. N. Ugryumova, S. J. Matcher, and D. P. Attenburrow, "Measurement of bone mineral density via light scattering," Phys. Med. Biol. **49**, 469–483 (2004).

45. G. Alexandrakis, F. R. Rannou, and A. F. Chatziioannou, "Tomographic bioluminescence imaging by use of a combined optical-PET (OPET) system: a computer simulation feasibility study," Phys. Med. Biol. **50**, 4225–4241 (2005).

46. A. A. Kamshilin, E. Nippolainen, I. S. Sidorov, P. V. Vasilev, N. P. Erofeev, N. P. Podolian, and R. V. Romashko, "A new look at the essence of the imaging photoplethysmography," Sci. Rep. **5**, 10494 (2015).

47. C. E. Dunn, B. Lertsakdadet, C. Crouzet, A. Bahani, and B. Choi, "Comparison of speckleplethysmographic (SPG) and photoplethysmographic (PPG) imaging by Monte Carlo simulations and in vivo measurements," Biomed. Opt. Express **9**, 4306–4316 (2018).

48. R. Graaff, A. C. M. Dassel, W. G. Zijlstra, F. F. M. de Mul, and J. G. Aarnoudse, "How tissue optics influences reflectance pulse oximetry," in *Advances in Experimental Medicine and Biology* (Plenum, 1996), Vol. **388**, pp. 117–132.

49. I. Mizeva, I. Makovik, A. Dunaev, A. Krupatkin, and I. Meglinski, "Analysis of skin blood microflow oscillations in patients with rheumatic diseases," J. Biomed. Opt. **22**, 070501 (2017).

50. I. Mizeva, E. Zharkikh, V. Dremin, E. Zherebtsov, I. Makovik, E. Potapova, and A. Dunaev, "Spectral analysis of the blood flow in the foot microvascular bed during thermal testing in patients with diabetes mellitus," Microvasc. Res. **120**, 13–20 (2018).

51. A. P. Popov, A. V. Bykov, and I. V. Meglinski, "Influence of probe pressure on diffuse reflectance spectra of human skin measured in vivo," J. Biomed. Opt. **22**, 110504 (2017).

52. I. Mizeva, E. V. Potapova, V. V. Dremin, E. A. Zherebtsov, M. A. Mezentsev, V. V. Shupletsov, and A. V. Dunaev, "Optical probe pressure effects on cutaneous blood flow," Clin. Hemorheol. Microcirc. **72**, 259–267 (2019).

53. G. Zonios, U. Shankar, and V. K. Iyer, "Pulse oximetry theory and calibration for low saturations," IEEE Trans. Biomed. Eng. **51**, 818–822 (2004).

54. M. Nitzan, A. Romem, and R. Koppel, "Pulse oximetry: fundamentals and technology update," Med. Dev. Evidence Res. **7**, 231–239 (2014).

55. C. E. East and P. B. Colditz, "Intrapartum oximetry of the fetus," Anesth. Analg. **105**, S59–S65 (2007).

56. I. Fine, "Glucose correlation with light scattering patterns," in *Handbook of Optical Sensing of Glucose in Biological Fluids and Tissues* (Taylor & Francis, 2009), pp. 237–280.